Copyright © 1975 American Telephone and Telegraph Company
THE BELL SYSTEM TECHNICAL JOURNAL
Vol. 54, No. 4, April 1975
Printed in U.S.A.

Aluminum Oxide/Silicon Dioxide, Double-Insulator, MOS Structure

By J. T. CLEMENS, E. F. LABUDA, and C. N. BERGLUND

(Manuscript received May 15, 1974)

A double-insulator structure consisting of 500 Å of vapor-deposited Al_2O_3 and 1000 Å of thermally grown SiO_2 is used as the gate dielectric in a beam-lead-compatible, p-channel, MOSFET, silicon-integrated-circuit technology. The Al_2O_3 layer, in addition to serving as a sodium barrier and thereby providing a self-passivated technology, results in a positive flatband voltage shift when compared to an SiO_2 structure. The mechanism for this flatband voltage shift is the subject of this paper.

The major experimental results obtained are (i) a negative charge exists near the Al_2O_3/SiO_2 interface, its magnitude being independent of the Al_2O_3 thickness but inversely proportional to the SiO_2 thickness, (ii) the magnitude of the SiO_2/Si interface charge is inversely proportional to the SiO_2 thickness, and (iii) a potential jump of about 1.25 volts in flatband voltage is associated with the addition of the Al_2O_3 layer.

A physical model is proposed which assumes the existence of a constant voltage drop across the SiO_2 layer during the Al_2O_3 deposition and a corresponding charge buildup at the SiO_2/Al_2O_3 interface.

I. INTRODUCTION

The threshold voltage of an insulated-gate, field-effect transistor is directly dependent upon the properties of the gate insulator. A double-dielectric gate structure consisting of nominally 500 Å of vapor-deposited Al_2O_3 and 1000 Å of thermally grown SiO_2 is the basis of a beam-lead-compatible, *p*-channel, MOSFET, silicon-integrated-circuit technology.[1–3] The Al_2O_3 layer serves two functions. First, it is a diffusion barrier for light ions, such as sodium, and thus provides a self-passivated technology. Second, the Al_2O_3 layer shifts the threshold voltage of the MOS transistor in the positive direction (due to a flatband voltage shift). For example, for a ⟨100⟩ oriented, *n*-type, 10-ohm-cm, silicon substrate, a flatband voltage of 0.0 volt is obtained with the dual-dielectric structure and a titanium metal gate, characteristic of the beam-lead metallization system, whereas with just an SiO_2 structure the flatband voltage is −0.8 volt. The more positive

flatband voltage capability provided by the Al_2O_3 layer implies that MOSFET integrated circuits can be fabricated which have low power-dissipation properties and which are more easily interfaced with bipolar circuits.

Many techniques have been used for the deposition of Al_2O_3 films intended for application in an integrated-circuit technology. All of our considerations are restricted to Al_2O_3 films deposited at 900°C from an $AlCl_3$ source, the technique reported by Tung and Caffrey.[1] A brief review is given in Ref. 4 of the other Al_2O_3 deposition techniques that have been reported and the electrical characteristics of the films obtained.

The electrical properties of the Al_2O_3/SiO_2, dual-dielectric, gate insulator are quantitatively described in this paper; and, in particular, the mechanisms are delineated which cause the positive shift in flatband voltage. The experimental approach was to do a parametric study of the flatband voltage of the dual-dielectric MOS structure, the two parameters of interest being the thicknesses of the Al_2O_3 and SiO_2 layers.

Two major conclusions were obtained from the parametric study. First, a net negative charge exists near the Al_2O_3/SiO_2 interface, and the magnitude of the charge is independent of Al_2O_3 thickness over the range studied, but inversely proportional to SiO_2 thickness. Second, the magnitude of the normal interface charge associated with the SiO_2/Si interface has a component that is inversely proportional to SiO_2 thickness.

A model explaining the origin of the negative charge at the $Al_2O_3/$ SiO_2 interface was developed, based on the assumption that the electrical conductivity of Al_2O_3 at high temperatures ($>300°C$) is much greater than that of SiO_2. As a result, during the high-temperature deposition of Al_2O_3, an electric field exists in the SiO_2 due to the Si/Al_2O_3 contact potential difference, and the negative charge at the Al_2O_3/SiO_2 interface terminates this field.

Recently, Aboaf, Kerr, and Bassous also reported the existence of a negative charge at the Al_2O_3/SiO_2 interface with the magnitude of the charge being independent of the Al_2O_3 thickness and inversely proportional to the SiO_2 thickness.[4] This is consistent with the insulator interface charge origin model we proposed[5] and implies that this model has general applicability in dual-dielectric structures, since they used three Al_2O_3 deposition techniques, all different from the technique used to obtain the Al_2O_3 films studied in this paper.

The organization of the paper is as follows. A simple flatband theory for dielectric structures is presented in Section II and space-charge formation in insulators is discussed in Section III. A theoretical

discussion of the Al_2O_3/SiO_2 structure is given in Section IV and the experimental results are presented in Section V. A summary is given in Section VI.

II. FLATBAND CALCULATIONS

The flatband voltage of an MOS structure is defined as that voltage which must be applied to the metal electrode to produce a zero space charge or flatband condition in the semiconductor, and it is determined by the net charge density existing in the insulator system and the various interfacial barrier energies. To calculate the flatband voltage, the voltage across the insulators under flatband conditions is calculated from the net charge density using Gauss' law, and to this is added the voltage contributed by the various barrier energies.

Consider the band diagrams of the metal/SiO_2/Si and metal/Al_2O_3/SiO_2/Si systems shown in Figs. 1 and 2, respectively. The various barrier energies for these systems are defined in the figures. We shall assume that at the SiO_2/Si interface in both structures there is an interface charge layer Q_{ss}. The net charge density in the bulk of the SiO_2 is assumed to be zero and the charge density in the Al_2O_3 is denoted by $\rho_A(x)$. Using S.I. to denote the single-insulator system and D.I. the double-insulator system, it follows that the voltages across the insulators, V_i, due to the charge densities can be written as:

$$V_i(\text{S.I.}) = (Q_{ss}/\epsilon_{ox})T_{ox} \tag{1}$$

$$\begin{aligned} V_i(\text{D.I.}) &= Q_{ss}\left[\frac{T_{ox}}{\epsilon_{ox}} + \frac{T_A}{\epsilon_A}\right] + \int_{T_{ox}}^{T_A+T_{ox}} \frac{dx}{\epsilon_A} \int_0^x \rho_A(x')dx' \\ &= Q_{ss}\left[\frac{T_{ox}}{\epsilon_{ox}} + \frac{T_A}{\epsilon_A}\right] + \int_{T_{ox}}^{T_{ox}+T_A} \frac{T_{ox} + T_A - x}{\epsilon_A} \rho_A(x)dx, \end{aligned} \tag{2}$$

where $(\epsilon_{ox}, \epsilon_A)$, (T_{ox}, T_A) = the dielectric constants and thicknesses of the SiO_2 and Al_2O_3, respectively. In particular, $\epsilon_{ox} = 3.9$; $\epsilon_A = 9.0$.

The applied voltage difference between the metal and the semiconductor, the flatband voltage V_{FB}, for both structures can be written as:

$$V_{FB}(\text{S.I.}) = -(Q_{ss}/\epsilon_{ox})T_{ox} + (\phi_{m,ox} - \phi_B - \phi_f) \tag{3}$$

$$V_{FB}(\text{D.I.}) = -V_i(\text{D.I.}) + (\phi_{m,A} + \phi_{ii} - \phi_B - \phi_f). \tag{4}$$

The insulator-insulator barrier ϕ_{ii} is assumed to be positive if it is as shown in Fig. 2.

Consider the contact potential terms in eqs. (3) and (4). If we let W and χ with the appropriate subscripts denote the vacuum work functions and electron affinities, respectively, of the various materials, and, if we assume that the energy band matching between two different

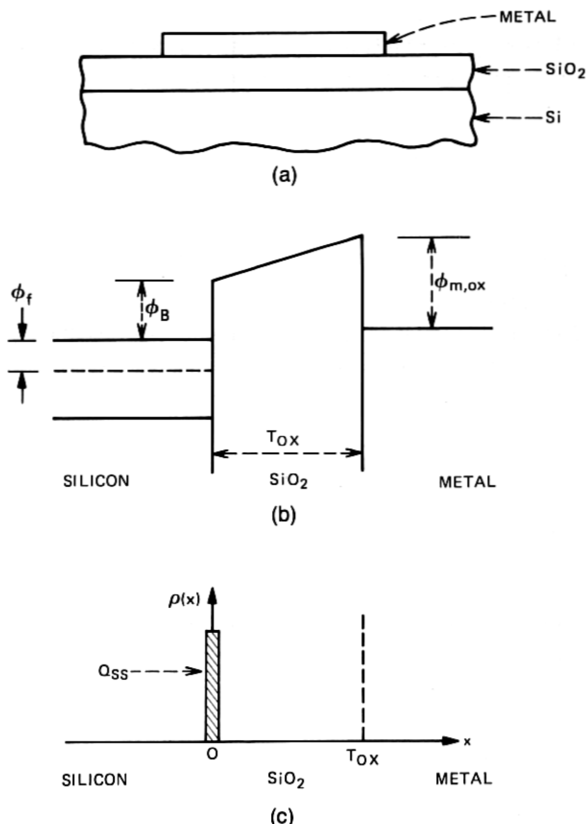

Fig. 1—(a) Cross-sectional view of the metal/SiO_2/Si capacitor structure. (b) Band diagram associated with the structure. (c) Plot of assumed charge density present in the structure.

materials is determined entirely by the difference in vacuum work functions, that is,

$$\phi_{m,ox} = W_m - \chi_{ox} \quad \text{and} \quad \phi_B = \chi_s - \chi_{ox}, \tag{5a}$$

then

$$\phi_{m,ox} - \phi_B - \phi_f = (W_m - \chi_{ox}) - (\chi_s - \chi_{ox}) - \phi_f = W_m - \chi_s - \phi_f, \tag{5b}$$

$$\phi_{m,A} + \phi_{ii} - \phi_B - \phi_f = (W_m - \chi_A) + (\chi_A - \chi_{ox}) - (\chi_s - \chi_{ox}) - \phi_f = W_m - \chi_s - \phi_f, \tag{6}$$

or

$$\phi_{m,ox} - \phi_B - \phi_f = \phi_{m,A} + \phi_{ii} - \phi_B - \phi_f = W_m - \chi_s - \phi_f. \tag{7}$$

Note that under this assumption, the contact potential terms are independent of the electron affinities of the insulators and dependent

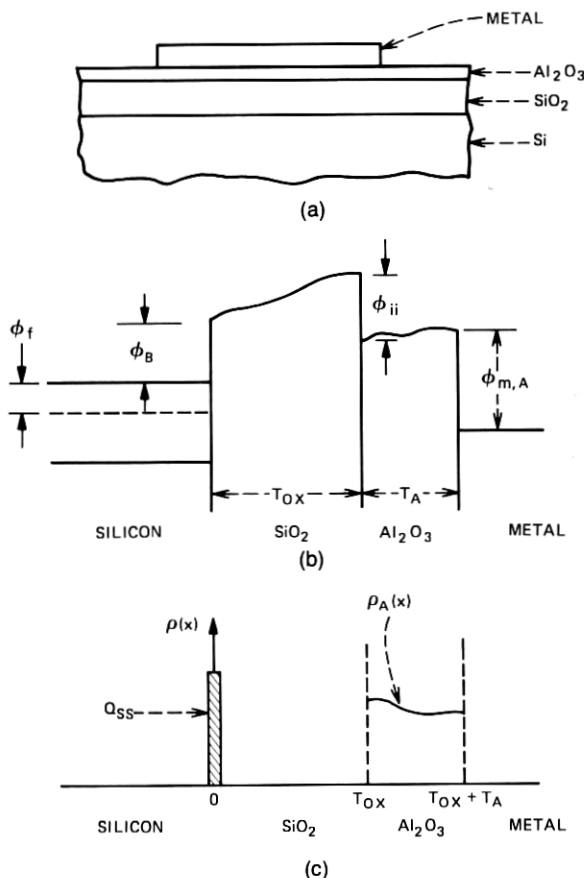

Fig. 2—(a) Cross-sectional view of the metal/Al_2O_3/SiO_2/Si capacitor structure. (b) Band diagram associated with the structure. (c) Plot of assumed charge density present in the structure.

only on the difference between the metal and semiconductor work functions. Thus, if the work-function assumption is valid, an MOS system involving a given metal and a semiconductor will have a constant flatband voltage after correction for Q_{ss} independent of the number or nature of the insulators, unless space charge exists in the insulators. In other words, if the assumption is valid, a measured V_{FB} that changes when the insulators are changed implies space charge exists in the insulators.

III. SPACE-CHARGE FORMATION IN INSULATORS

In the previous section, the flatband voltage of a dual-dielectric MOS structure was calculated assuming a given distribution of space charge. The purpose of this section is to discuss one possible model

for the origin and spatial location of space charge in insulators, namely, the one we feel represents the most likely explanation for much of the space charge in the SiO_2/Al_2O_3 system. In this discussion, we first summarize the proposal for space-charge formation suggested by Simmons for a metal-insulator-metal (MIM) system.[6] Then this model is extended and applied to double-insulator systems, in particular those using SiO_2 and Al_2O_3.

Suppose we form the MIM system shown in Fig. 3a at sufficiently low temperatures that no charge transport occurs within the insulator and no charge exchange occurs between the insulator and the metallic contacts in a time period comparable to the experimental observation time. In this case, no space charge can form in the insulator because thermal equilibrium will not exist and the potential versus position will look as shown in Fig. 3b, where the insulator is represented essentially as a wideband insulator with conduction and valence band edges. Now assume that the system is heated to a sufficiently high temperature that charge transport can occur within the insulator and charge exchange can occur between the insulator and the metallic contacts in a time period that is short compared to experimental observation. In this case, thermal equilibrium will be established and there will be two extreme possibilities between which the system will equilibrate: either the characteristic length corresponding to a space-charge region at thermal equilibrium in the insulator, the electrostatic screening, or Debye length will be large compared to the insulator thickness, and the potential versus position will be virtually identical to that shown in Fig. 3b; or the Debye length in the insulator will be small compared to the insulator thickness, and such space-charge regions as shown in Fig. 3c will form near the two metal interfaces. In the latter alternative, a well-defined "Fermi level" will exist in the bulk of the insulator, as shown in Figure 3c, which will coincide in energy with the Fermi level in the metallic contacts in much the same way that Fermi levels coincide in a conventional Schottky barrier on a semiconductor. Clearly an MIM system in which the Debye length is short compared to the insulator thickness at any given time will always lie somewhere between the extremes indicated in Figs. 3b and 3c, depending on thermal history, so that in such an insulator, space-charge regions will always exist in the vicinity of the metallic contacts. The magnitude of the charge will depend on the difference in the work function of the metal and the insulator and on the degree of thermal equilibrium which has been established.

In the above discussion, it has been assumed that there is no net voltage difference across the MIM structure. Very similar arguments can be presented for the case where a finite voltage exists between

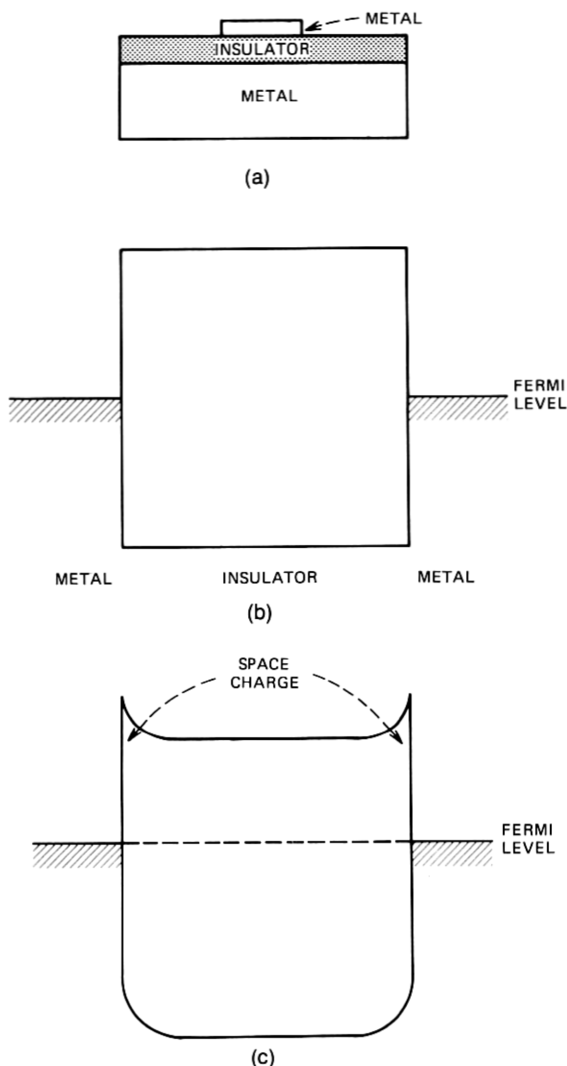

Fig. 3—(a) Cross-sectional view of a metal/insulator/metal capacitor structure. (b) Band diagram of the sturcture if the insulator Debye length is assumed to be much greater than the thickness of the insulator. (c) Band diagram of the structure if the insulator Debye length is assumed to be smaller than the thickness of the insulator.

the two metal contacts; the voltage is either applied or is due to differences in the two involved metal/insulator potential barrier heights. Assuming an insulator which forms space-charge regions that are narrow compared to the insulator thickness, the initial

potential diagram is shown dotted in Fig. 4a and the final steady-state situation is shown as the solid lines. The only electric field required in the bulk of the insulator under steady-state conditions is the ohmic field associated with any current injected from the electrodes, typically a negligible field.

Now suppose that the voltage is reduced as shown at $t = 0$ in Fig. 4b. Initially, the same space-charge that exists under applied voltage

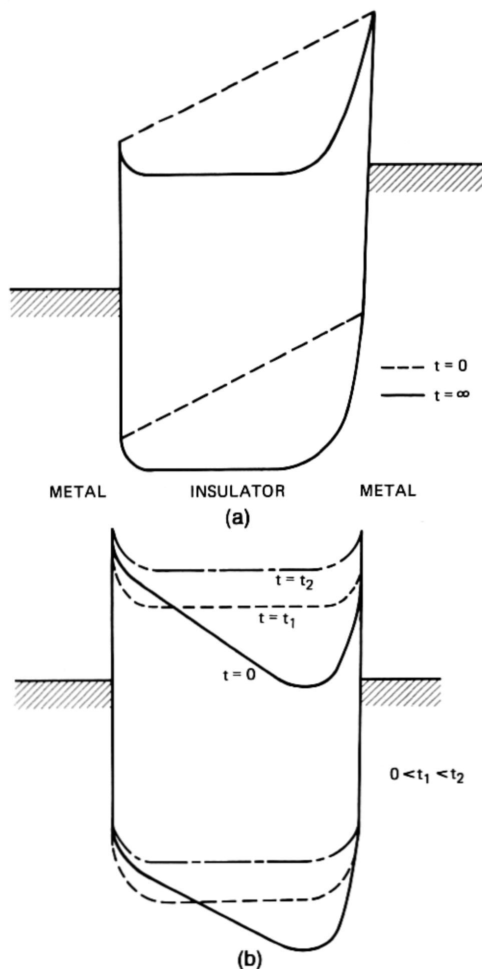

Fig. 4—(a) Band diagram of a metal/insulator/metal structure, whose insulator Debye length is less than the insulator thickness, depicting the immediate and equilibrium band structure in response to the application of an external voltage. (b) Band diagram of the same structure depicting the time response of the bands after the applied voltage is reduced to zero.

will remain. After a time t_1 at elevated temperature, there will be a redistribution of charge as shown, the total amount of charge remaining fixed. Finally, if the temperature is further raised or after an additional time t_2, carriers will be injected from one or both electrodes to bring the system to the equilibrium of Fig. 3c.

The above argument for space-charge formation in insulators is an especially powerful one because it invokes well-known concepts. It simply applies the concepts of steady state, thermal equilibrium, and Fermi level to insulators and shows that the important features of space-charge layers in insulators can be described in terms of only one parameter, the work function or Fermi level position in the insulator at thermal equilibrium. (A more detailed discussion is available in the work of Simmons.[6]) With this as a starting point, it is possible to discuss a wide variety of charging phenomena in insulating thin films in an intuitively understandable way; and it should provide a basis for more quantitative analyses of a number of such effects. In the following section, the concepts discussed here are applied to the silicon/SiO_2/Al_2O_3/metal structure with emphasis on the space-charge region that builds up near the insulator/insulator interface during deposition of the Al_2O_3.

IV. THE SiO_2/Al_2O_3 SYSTEM MODEL

The concepts of the preceding section can be applied to the double-layer structure shown in Fig. 2 in which the first layer is SiO_2 and the second is Al_2O_3. Previous experimental results have indicated that the density of trap levels in thermally grown SiO_2 is sufficiently low that the Debye length should be much larger than the typical SiO_2 film thickness of a few thousand Angstroms.[7] This supports the assumption made previously that no finite charge density exists in the bulk of the SiO_2 film. On the other hand, the trap density in deposited Al_2O_3 films has been found to be much larger so that it is reasonable to assume that the Debye length is small compared to the Al_2O_3 film thicknesses that we will consider.[8–10] The Al_2O_3 films of interest are deposited at 900°C. The double-insulator system is assumed to be at an elevated temperature during the deposition for a sufficient length of time that thermal equilibrium will be established, and under these conditions, the potential diagram versus position will be like that shown in Fig. 5. Since the Fermi level in the silicon must coincide with that in the Al_2O_3 at thermal equilibrium, a contact potential difference will exist that will result in (*i*) an electric field in the SiO_2, (*ii*) a space-charge region in the Si at the Si/SiO_2 interface, (*iii*) a space-charge region in the Al_2O_3 at the SiO_2/Al_2O_3 interface, and (*iv*) zero electric field in the bulk of the Al_2O_3 film. In addition, depending on the Al_2O_3 surface boundary

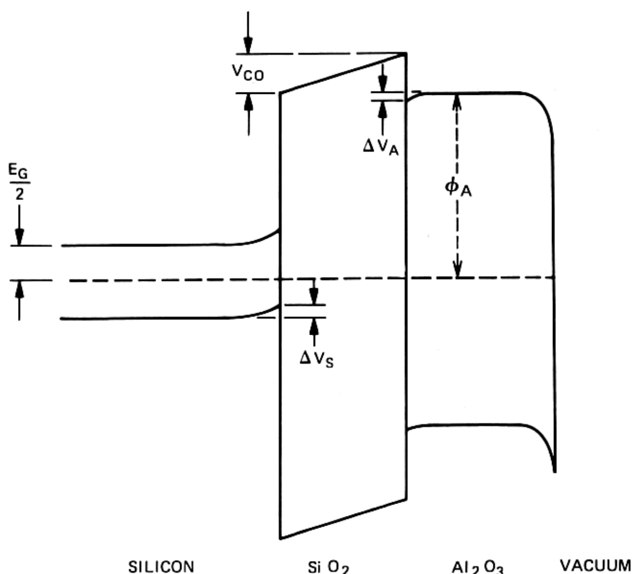

Fig. 5—Band diagram of the $Al_2O_3/SiO_2/Si$ system in equilibrium at high temperature.

conditions, a space-charge region may exist near the outer Al_2O_3 surface.

The important parameter in the SiO_2/Al_2O_3 system is the total potential difference V_c that must build up to align the Fermi levels in the silicon and the Al_2O_3. This potential difference will be made up of a potential V_{co} across the SiO_2 and the drops in potential due to the band-bending regions in the silicon near the Si/SiO_2 interface and in the Al_2O_3 near the SiO_2/Al_2O_3 interface, ΔV_s and ΔV_A, respectively (see Fig. 5). That is,

$$V_c = V_{co} + \Delta V_s + \Delta V_A, \tag{8a}$$

where the system equilibrium condition is given by

$$(E_G/2) + \phi_B + V_c - \phi_{ii} - \phi_A = 0. \tag{8b}$$

If it is assumed that the work function argument applies to the SiO_2/Al_2O_3 system, then

$$V_c = \chi'_A + \phi_A - \chi'_s - (E_G/2), \tag{9}$$

where χ'_A is the Al_2O_3 electron affinity at the deposition temperature; ϕ_A is the energy separation between the Al_2O_3 conduction band and the Fermi level in the bulk; χ'_s is the silicon electron affinity; and the $E_G/2$ term represents the assumption that the silicon is intrinsic at the elevated temperature of interest.

Since the electric field in the SiO_2 is determined directly by the potential drop V_{co} and the oxide thickness T_{ox}, the net charge present in the narrow space-charge region at the Al_2O_3/SiO_2 interface is given by

$$Q_{ii} = (\epsilon_{ox}/T_{ox})\{V_c - \Delta V_s - \Delta V_A\}. \tag{10}$$

Over a wide range of SiO_2 thickness, ΔV_s and ΔV_A will be negligible compared to V_c. For example, even assuming that V_{co} corresponds to an electric field in the SiO_2 of 10^6 volts/cm, ΔV_s is less than 0.1 volt at 900°C.* Thus, eq. (10) can be approximated by

$$Q_{ii} = (\epsilon_{ox}/T_{ox})V_c \approx \epsilon_{ox}/T_{ox}\{\chi_A' + \phi_A - \chi_s' - (E_G/2)\}. \tag{11}$$

From eqs. (10) and (11), several interesting properties of Q_{ii} are apparent. First, its magnitude is relatively independent of the quality and reproducibility of the Al_2O_3 provided only that $\phi_A + \chi_A'$ is reproducible and ΔV_A is negligible. The band-bending ΔV_A may vary markedly from sample to sample depending on the trap density, but as long as the space-charge region is relatively narrow so that ΔV_A is small compared to V_c, this variation will have no significant effect. Second, the magnitude of Q_{ii} varies inversely with the SiO_2 thickness T_{ox} and is independent of Al_2O_3 thickness T_A. This effect provides a straightforward and unique prediction of the model that can easily be tested experimentally.

If the system is now cooled to room temperature, the conductivity of the Al_2O_3 will be reduced to the point where the space-charge regions will not move or change under application of an electric field for long periods of time, and these regions will be effectively frozen in. We must consider the two possible space-charge regions in the Al_2O_3, one at the Al_2O_3/SiO_2 interface, and the other at the outer surface. The contributions V_{ii} and V_m, respectively, of these charge layers to the flatband voltage is given by (see eq. 2)

$$V_{ii} = -\int_{T_{ox}}^{T_{ox}+T_A} \left[\frac{T_{ox} + T_A - x}{\epsilon_A}\right] \rho_{ii}(x)dx = -\frac{T_A}{\epsilon_A} Q_{ii} \tag{12}$$

and

$$V_m = -\int_{T_{ox}}^{T_{ox}+T_A} \left[\frac{T_{ox} + T_A - x}{\epsilon_A}\right] \rho_m(x)dx, \tag{13}$$

where $\rho_{ii}(x)$ and $\rho_m(x)$ are the net charge densities at the SiO_2/Al_2O_3 and Al_2O_3/metal interfaces, respectively. In the limit where $\rho_{ii}(x)$ is located in a plane at the interface, an effective interface charge density Q_{ii} is defined by eq. (12). The term V_m is a constant independent

*This can be shown from an integration of Poisson's equation and using the fact that at 900°C the intrinsic charge density in the silicon is approximately 10^{19} cm^{-3}.

of T_{ox} and T_A if $\rho_m(x)$ is a function only of the distance $(T_{ox} + T_A - x)$ between the charge and the metal. Combining (2), (11), (12), and (13) gives for the flatband voltage of the double-insulator structure

$$V_{FB}(\text{D.I.}) = (\phi_{m,A} + \phi_{ii} - \phi_s) + V_m - Q_{ss}\left[\frac{T_{ox}}{\epsilon_{ox}} + \frac{T_A}{\epsilon_A}\right] - V_c \frac{\epsilon_{ox} T_A}{\epsilon_A T_{ox}}, \quad (14)$$

and, for completeness, the flatband voltage of the single insulator [eq. (3)] is

$$V_{FB}(\text{S.I.}) = (\phi_{m,ox} - \phi_s) - \frac{Q_{ss}}{\epsilon_{ox}} T_{ox}, \quad (15)$$

where $\phi_s = \phi_B + \phi_f$.

V. EXPERIMENTAL RESULTS

5.1 Preliminary remarks

Dual-dielectric MIS capacitor structures with various insulator thicknesses were fabricated on n- and p-type silicon substrates with resistivities of approximately 10 ohm-cm. For the n-type substrates both ⟨100⟩ and ⟨111⟩ orientations were investigated. The SiO_2 was thermally grown at 1100°C using oxygen bubbled through 80°C water as the ambient. The Al_2O_3 was vapor deposited on the SiO_2 at 900°C from an $AlCl_3$ source. The details of the Al_2O_3 deposition process are given in Ref. 1. The insulator thicknesses, T_{ox} and T_A, were varied by varying the growth and deposition times of the SiO_2 and the Al_2O_3, respectively.

The deposition of the Al_2O_3 duplicated exactly the procedure used for fabricating integrated circuits. As such, a layer of SiO_2 was also deposited on top of the Al_2O_3, which in the fabrication of integrated circuits is used as an etch mask for defining patterns in the Al_2O_3 film. For our samples, this layer of SiO_2 was chemically stripped prior to any measurements or any further processing.

One feature that may be important in this study is the method of formation of the metal electrodes. Depending on the deposition technique used, the samples may be heated for a sufficient time during the metal deposition to form a space-charge region at the Al_2O_3/metal interface. However, if this induced space charge is reproducible and constant from sample to sample and is spatially constrained to a region very near the interface, it will only influence the flatband voltage via the constant voltage term V_m in (14). Experimentally, we shall attempt to assure the reproducibility of this possible space-charge effect by measuring the MIS structures at room temperature with a

mercury electrode.[11] Several samples were also investigated with thermally evaporated titanium-aluminum electrodes.

Initially, we attempted to vary the Al_2O_3 thickness by etching in discrete steps rather than by varying the deposition time. This approach was abandoned because of nonuniform etching of the Al_2O_3. In Fig. 6, scanning electron micrographs are given of the surface of the Al_2O_3 as deposited and after etching a portion of the layer. Microscopic thickness variations (± 500 Å) are evident after etching. Since these variations lead to significant errors in the flatband voltage measurements, the Al_2O_3 thickness was varied only by varying the growth time.

Experimental data for each sample investigated were obtained by means of high-frequency capacitance-voltage (C–V) analysis.[12] Such measurements, obtained using either the mercury probe electrode or thermally evaporated titanium-aluminum thin-film electrodes, enable one to obtain accurate measurements of the insulator thickness and

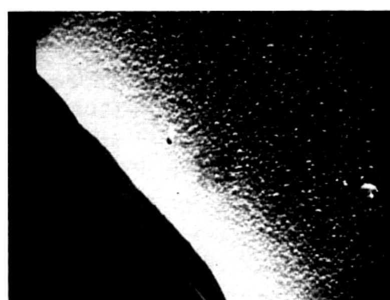

AS DEPOSITED
$T_A \approx 1750$ Å

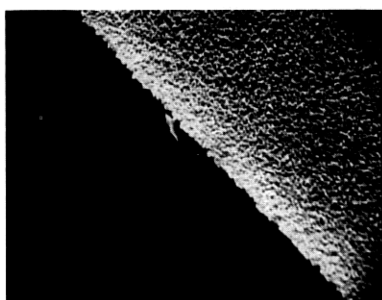

5 MIN ETCH–BACK
$T_A \approx 1250$ Å

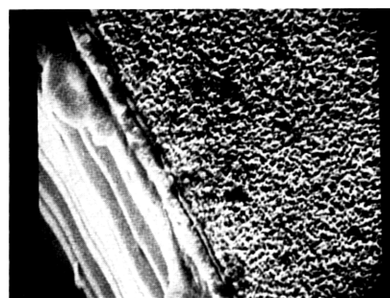

12 MIN ETCH–BACK
$T_A \approx 500$ Å

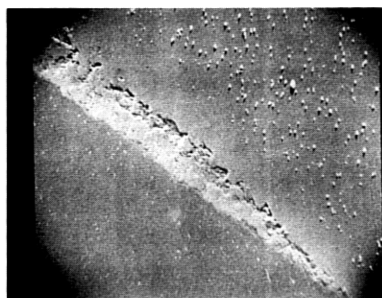

17 MIN ETCH–BACK
$T_A \approx 0$ Å

Fig. 6—SEM photographs depicting the increasing roughness of the Al_2O_3 surface as it is etched back using phosphoric acid.

the associated flatband voltage. Each data point reported is the average flatband voltage calculated from at least three measurements performed on each sample. The typical spread in measurements is 0.10 volt. When measurements are performed on the double-insulator (Al_2O_3/SiO_2) structure, a measurement of V_{FB}(D.I.) [eq. (14)] is obtained. The normalized accumulation capacitance C_{acc} (farads/cm^2), which is a measure of the insulator thicknesses, is given by

$$C_{acc}(\text{D.I.}) = \left[\frac{T_{ox}}{\epsilon_{ox}} + \frac{T_A}{\epsilon_A} \right]^{-1}. \quad (16)$$

When the Al_2O_3 is completely etched off and C–V analysis is conducted on the remaining single insulator (SiO_2), then measurements of V_{FB}(S.I.) [see eq. (15)] are obtained. The normalized accumulation capacitance in this case yields a measurement of T_{ox} since

$$C_{acc}(\text{S.I.}) = \frac{\epsilon_{ox}}{T_{ox}}. \quad (17)$$

By combining eqs. (16) and (17), accurate measurements of both T_A and T_{ox} are obtained.

It is possible to obtain independent quantitative values for Q_{ss} for each sample studied after the Al_2O_3 is etched off if the constant term $(\phi_{m,ox} - \phi_s)$ in eq. (14) is known. Measurement of $(\phi_{m,ox} - \phi_s)$ can be accomplished by SiO_2 etch-back experiments in which V_{FB}(S.I.) is measured as the SiO_2 layer is successively thinned by etching in a dilute hydrofluoric acid solution. Typical data obtained with a mercury probe on four different samples are shown in Fig. 7. As expected, there is a linear relationship between V_{FB}(S.I.) and T_{ox} and an extrapolation of this relationship back to $T_{ox} = 0$ indicates that 0.67 volt is the appropriate value of $(\phi_{m,ox} - \phi_s)$ for n-type, 10-ohm-cm Si and a mercury electrode. This value is in excellent agreement with previously determined values.[13] The experiment also provides independent verification of the assumption that there is negligible space charge in the bulk of the SiO_2.

Based upon the value of Q_{ss} for each sample, it is possible to characterize the flatband voltage shift due to the Al_2O_3. Correcting for the Q_{ss} term and, additionally, subtracting the constant term $(\phi_{m,ox} - \phi_s)$ from eq. (14), a corrected differential flatband voltage ΔV_{FB} can be defined as:

$$\Delta V_{FB} = V_{FB}(\text{D.I.}) - (\phi_{m,ox} - \phi_s) + Q_{ss}\left[\frac{T_{ox}}{\epsilon_{ox}} + \frac{T_A}{\epsilon_A} \right]$$
$$= (\phi_{m,A} + \phi_{ii} - \phi_{m,ox}) + V_c\left(\frac{\epsilon_{ox}}{\epsilon_A}\right)\left(\frac{T_A}{T_{ox}}\right) + V_m. \quad (18)$$

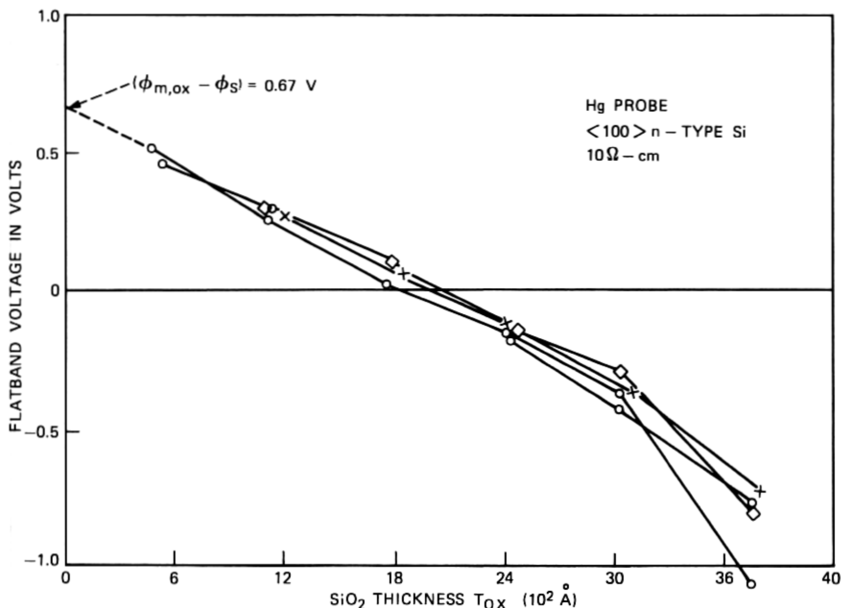

Fig. 7—Plot of the $Hg/SiO_2/Si$ flatband voltage for four wafers as a function of the SiO_2 thickness. Data obtained from SiO_2 etch-back experiments on 10-ohm-cm, n-type, ⟨100⟩, Si substrates.

5.2 Results pertaining to Q_{ii}

Experimental values of V_{FB}(D.I.) for the dual-insulator structure are plotted in Fig. 8 as a function of the Al_2O_3 thickness T_A for a SiO_2 thickness of $\approx$1200 Å on n-type, ⟨100⟩ substrates. These results were obtained with a mercury electrode. Although there is considerable scatter in the data, it is clear that V_{FB}(D.I.) increases monotonically with increasing Al_2O_3 thickness which is in agreement with eq. (14) if the sign of V_c is such that a net negative charge exists at the SiO_2/Al_2O_3 interface. The experimental uncertainties in the V_{FB} measurements are estimated to be $\pm$0.05 volt. Correcting this data for Q_{ss} and subtracting $(\phi_{m,ox} - \phi_s)$, the results are replotted in Fig. 9. This refinement technique leads to a considerable reduction in the scatter in the data and demonstrates that ΔV_{FB} is a linear function of the Al_2O_3 thickness T_A, as predicted by eq. (18). The linear relationship also provides striking evidence that Q_{ii}, the negative charge at the Al_2O_3/SiO_2 interface, is constant from sample to sample for Al_2O_3 thicknesses in the range of 500 Å to 2500 Å if the SiO_2 thickness is held constant. This is in agreement with the postulated model and provides experimental verification of the assumption that the Debye length in Al_2O_3 is small compared to the Al_2O_3 thickness. Given that the Debye length

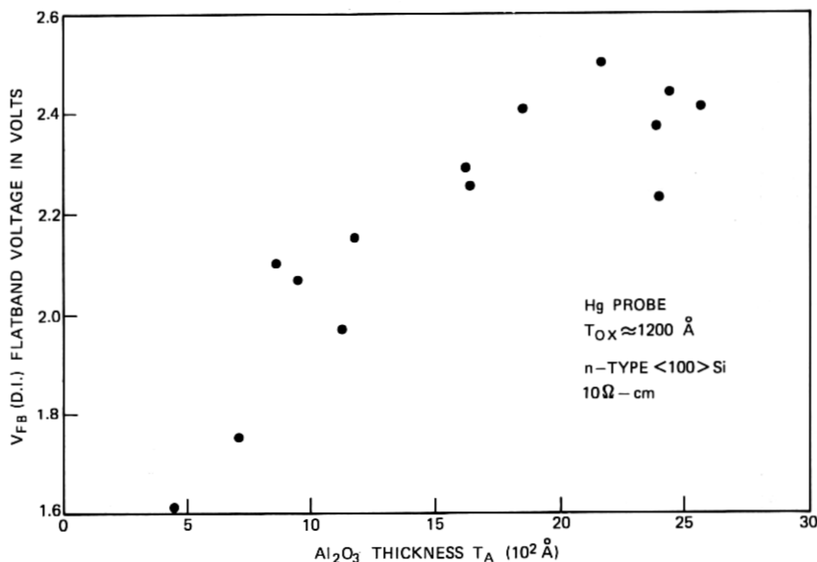

Fig. 8—Plot of the $Hg/Al_2O_3/SiO_2/Si$ flatband voltage as a function of the Al_2O_3 thickness for a constant SiO_2 thickness (T_{ox} = 1200 Å) on n-type, ⟨100⟩, Si substrates.

is small compared to 500 Å at 900°C, estimates of ΔV_A assuming charge densities in excess of 10^{18} cm^{-3} indicate that ΔV_A will be less than 0.1 volt and, thus, negligible as previously assumed.

The data presented so far proves that Q_{ii} is negative and a constant for fixed SiO_2 thickness independent of Al_2O_3 thickness. Another prediction of our model is that Q_{ii} is inversely proportional to the SiO_2

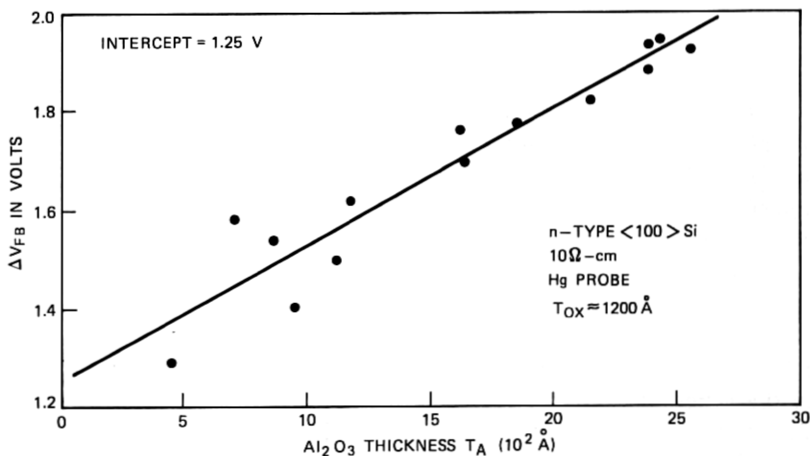

Fig. 9—Plot of the corrected differential flatband voltage as a function of the Al_2O_3 thickness for a constant SiO_2 thickness (T_{ox} = 1200 Å) on n-type, ⟨100⟩, Si substrates.

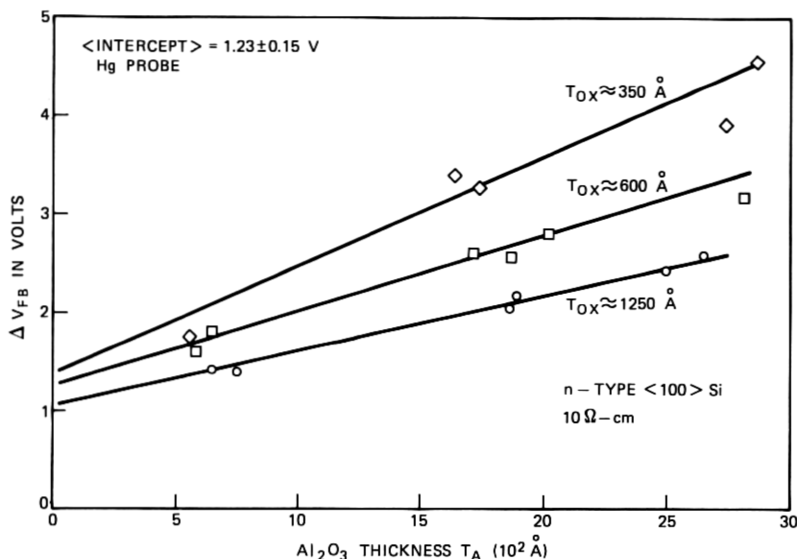

Fig. 10—Plot of the corrected differential flatband voltage as a function of the Al_2O_3 thickness for various values of SiO_2 thickness on *n*-type, ⟨100⟩, Si substrates.

thickness [eq. (11)]. That this is indeed the case is shown by the data presented in Figs. 10 and 11, which were obtained with a mercury probe and are for ⟨100⟩, *n*-type, silicon substrates. In Fig. 10, ΔV_{FB} is

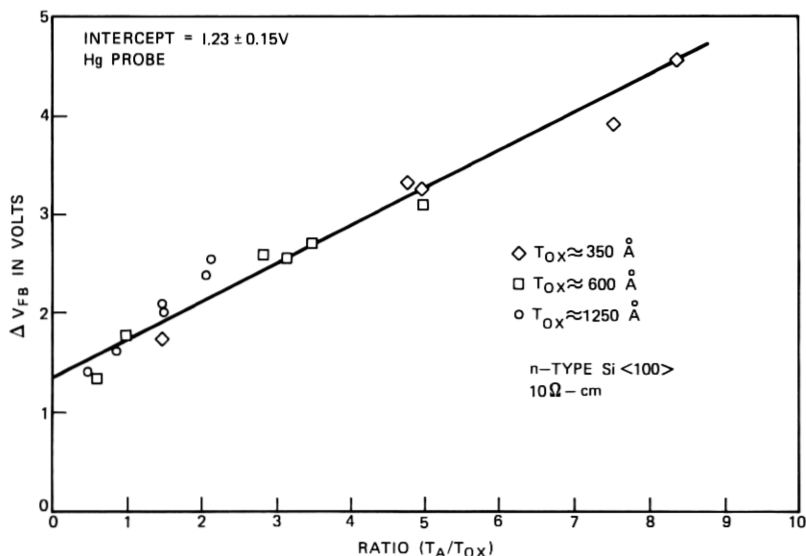

Fig. 11—Plot of the corrected differential flatband voltage as a function of the ratio of Al_2O_3 thickness to SiO_2 thickness on *n*-type, ⟨100⟩, Si substrates.

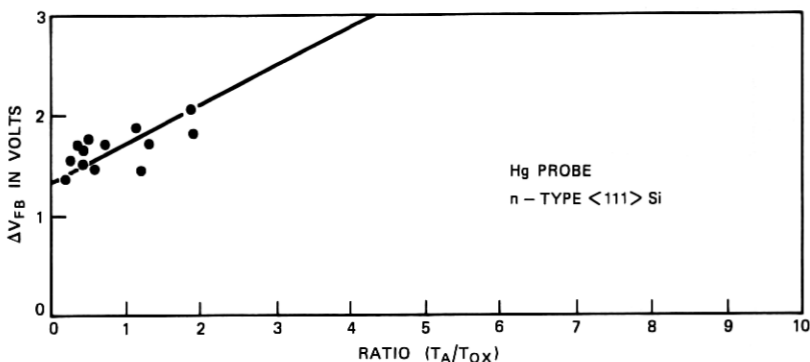

Fig. 12—Plot of the corrected differential flatband voltage as a function of the ratio of Al_2O_3 thickness to SiO_2 thickness on n-type, ⟨111⟩, Si substrates.

plotted versus Al_2O_3 thickness for three different SiO_2 thicknesses. In each case, a linear relationship between ΔV_{FB} and Al_2O_3 thickness is obtained, and the increased slope obtained with smaller SiO_2 thicknesses indicates that Q_{ii} does increase as the SiO_2 thickness is decreased. The data of Fig. 10 are replotted in Fig. 11 as a function of T_A/T_{ox}, the ratio of Al_2O_3 thickness to SiO_2 thickness. As expected from eq. (18), the ΔV_{FB} versus T_A/T_{ox} relationship is accurately represented by a straight line over the T_A/T_{ox} range investigated (0.5 to 8), indicating that Q_{ii} is inversely proportional to the SiO_2 thickness. The slope of the straight line in Fig. 11 corresponds to a V_c value of 0.88 volt.* This value for V_c was obtained in all the measurements on ⟨100⟩ substrates within ±0.1 volt.

Similar measurements were also performed with ⟨111⟩ oriented, n-type substrates. The larger values of Q_{ss} inherent in the ⟨111⟩ orientation meant that the Q_{ss} correction factor was much larger and, hence, the accuracy of the results was somewhat poorer. Results for ⟨111⟩ samples are given in Fig. 12, where ΔV_{FB} is plotted as a function of the T_A/T_{ox} ratio. Again these data were obtained with a mercury probe. The straight line shown in Fig. 12 is a best fit to the data if the slope of the line is restricted to correspond to a V_c value of 0.88 volt. Considering the possible errors due to the Q_{ss} correction, the straight-line fit of the data in Fig. 12 is good enough to conclude that the value of Q_{ii} is independent of the substrate orientation for the two orientations investigated, ⟨100⟩ and ⟨111⟩, and in complete agreement with the predictions of our model.

* For 1000 Å of SiO_2, a V_c value of 0.88 volt corresponds to a Q_{ii} value of 1.9×10^{11} charges/cm^2.

5.3 Results pertaining to Q_{ss}

All of the experimental results presented so far have focused on Q_{ii}, the charge at the Al_2O_3/SiO_2 interface. Some interesting facets of Q_{ss}, the charge at the SiO_2/Si interface, were also discovered during our study and are discussed in the following. As mentioned previously, a value of Q_{ss} was determined for all samples by measuring the flatband voltage V_{FB}(S.I.) of the single-insulator structure after removing the Al_2O_3 and then calculating Q_{ss} using the $(\phi_{m,ox} - \phi_s)$ value for the Hg/SiO_2/Si system as determined in Fig. 7. A plot of V_{FB}(S.I.) versus T_{ox}, the SiO_2 thickness, for n-type, ⟨100⟩ substrates is given in Fig. 13. Previous results published in the literature have shown that for single-insulator (SiO_2/Si) structures, Q_{ss} is independent of the SiO_2 thickness.[14] If this were the case for our structures, we would expect to find a linear relationship between V_{FB}(S.I.) and T_{ox} with an intercept on the V_{FB}(S.I.) axis equal to $(\phi_{m,ox} - \phi_s) = 0.67$ volt. The results given in Fig. 13 indicate that this is not the case. Although the data could be interpreted as being consistent with a linear relationship, they are definitely not consistent with an intercept equal to 0.67 volt. The results are more consistent with the supposition that, to first order, V_{FB}(S.I.) is independent of T_{ox}.

A more detailed study of Q_{ss} was pursued by preparing samples of various SiO_2 thicknesses (n-type, Si, ⟨100⟩) and measuring V_{FB}(S.I.) for each sample. Approximately 500 Å of Al_2O_3 was then deposited

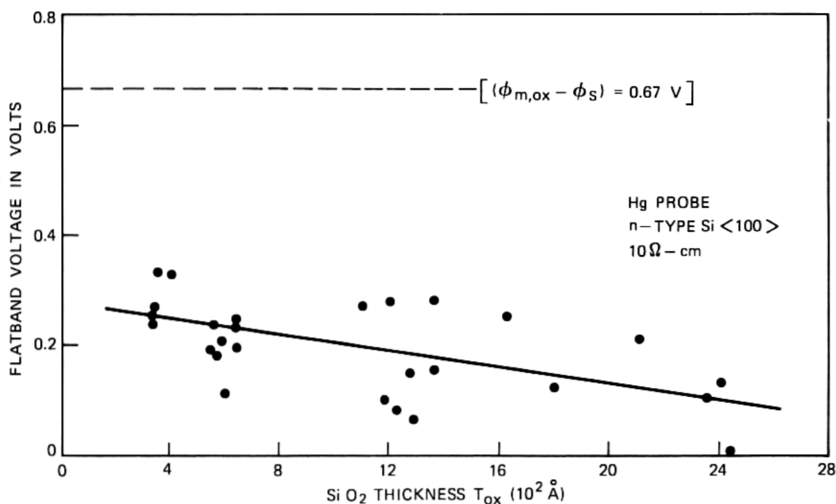

Fig. 13—Plot of the Hg probe single-insulator flatband voltage after Al_2O_3 deposition and etch-off as a function of SiO_2 thickness for n-type, ⟨100⟩, Si substrates.

on all samples, the Al_2O_3 was removed by etching, and V_{FB}(S.I.) was remeasured. Finally, for each of the samples, the SiO_2 was etched back in steps, and V_{FB}(S.I.) was determined as a function of SiO_2 thickness. The results are given in Fig. 14.

Prior to Al_2O_3 deposition, the results are consistent with the samples having a constant value of Q_{ss} independent of T_{ox}, that is, a linear relationship exists between V_{FB}(S.I.) and T_{ox} with an intercept equal to 0.67 volt. However, after Al_2O_3 deposition, V_{FB}(S.I.) is seen to be essentially independent of T_{ox}. Furthermore, if the SiO_2 is now etched back, a linear relationship between V_{FB}(S.I.) and SiO_2 thickness is obtained with an intercept equal to 0.67 volt. In Fig. 14, results of the etch-back study are given for only one representative sample, since the results obtained on the other samples were similar.

The conclusion which follows from the results given in Fig. 14 is that before the deposition of the Al_2O_3, Q_{ss} is independent of T_{ox}, whereas after deposition, the value of Q_{ss} is changed, the amount of change depending upon T_{ox}, the SiO_2 thickness. This effect is further illustrated by the results given in Fig. 15, where Q_{ss} after Al_2O_3 deposition and etch-off is plotted versus $1/T_{ox}$ for both ⟨100⟩ and ⟨111⟩, n-type substrates. For both orientations, the data are seen to fall

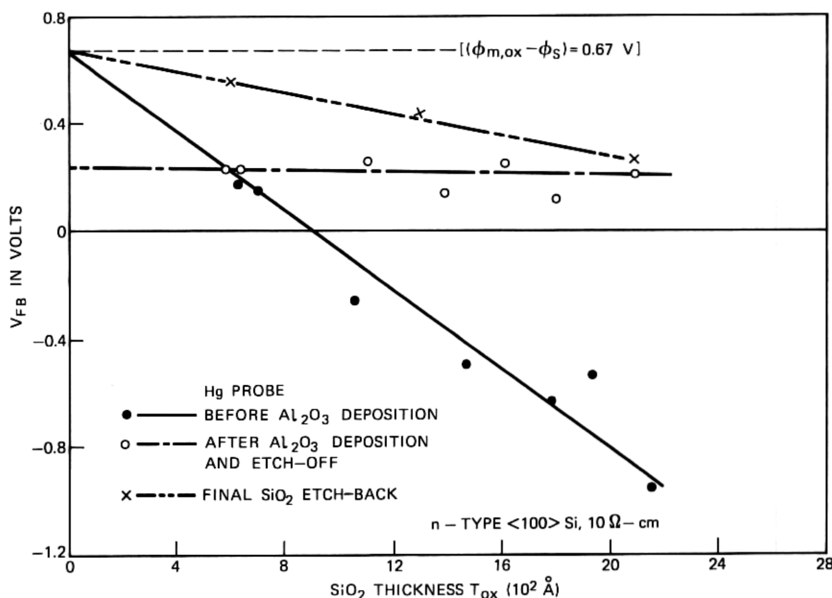

Fig. 14—Plot of the single-insulator flatband voltage before and after Al_2O_3 deposition and after final SiO_2 etch-back, indicating the change in Q_{ss} induced by the Al_2O_3 deposition on n-type, ⟨100⟩, Si substrates.

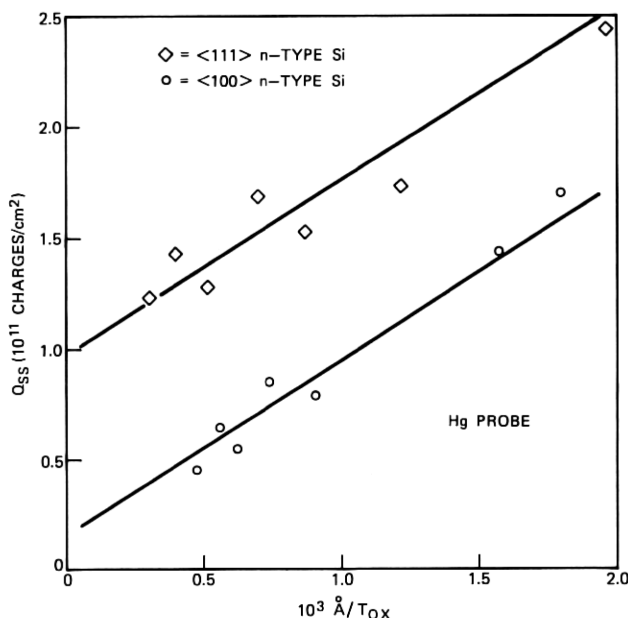

Fig. 15—Plot of Q_{ss} after Al_2O_3 deposition as a function of the SiO_2 thickness for n-type, ⟨100⟩ and ⟨111⟩, Si substrates.

along a straight line consistent with the equation

$$Q_{ss} = (v_o \epsilon_{ox}/T_{ox}) + Q_{sso}. \tag{19}$$

The slopes of the two lines in Fig. 15 were taken to be equal to each other ($v_o = 0.38$ volt), and it is observed that an excellent fit to the two sets of data is obtained with the one v_o value. The background charge densities, Q_{sso}, or equivalently the values of Q_{ss} for large values of T_{ox} are approximately 1.0×10^{11} and 1.0×10^{10} charges/cm^2 for ⟨111⟩ and ⟨100⟩ orientations, respectively. For the ⟨100⟩ orientation, Q_{sso} is negligible.

The results presented so far have established that for the double-insulator structure, both Q_{ii} and Q_{ss} depend on T_{ox} and that these dependencies can be written as:

$$\begin{aligned} Q_{ii} &= \epsilon_{ox} V_c / T_{ox} \\ Q_{ss} - Q_{sso} &= \epsilon_{ox} v_o / T_{ox}, \end{aligned} \tag{20}$$

where $V_c \simeq 0.88$ volt and $v_o \simeq 0.38$ volt. Thus, the single-insulator flatband voltage after Al_2O_3 deposition can be written as

$$V_{FB}(\text{S.I.}) = (\phi_{m,ox} - \phi_s) - v_o - (T_{ox}/\epsilon_{ox}) Q_{sso}, \tag{21}$$

which is consistent with the after-deposition results presented in Fig. 14. Considering Q_{sso} as a fundamental property of the SiO_2/Si interface, which is not affected by the Al_2O_3 deposition, it follows that the contribution to the single-insulator flatband voltage, δV_{FB}, induced by the portion of Q_{ss} that is influenced by the Al_2O_3 deposition is

$$\delta V_{FB} = v_o. \tag{22}$$

The voltage drop across the SiO_2 during the deposition of the Al_2O_3 is V_c, and if this is considered as a stress voltage applied to the SiO_2/Si interface, then

$$V_c(\text{stress})/\delta V_{FB} = \alpha = 2.3. \tag{23}$$

It is interesting to note that this result is in good agreement with previously published results relating stress voltage to saturated flatband voltage shift for SiO_2/Si structures. Specifically, in Ref. 15 it was observed that the ratio of stress voltage to saturated flatband voltage shift was given by:

$$\alpha = \begin{cases} 3.33 \text{ at } 350°\text{C} \\ 2.38 \text{ at } 450°\text{C}. \end{cases} \tag{24}$$

One implication of the relationship given in eq. 20 for Q_{ss} is that for ⟨100⟩ substrates, where Q_{sso} is negligible, the flatband voltage of a double-insulator structure will be insensitive to a SiO_2 thickness variation. Thus, in MOSFET integrated circuits with a ⟨100⟩ substrate, where a thick SiO_2 layer is used to inhibit parasitic inversion, the contribution of the Q_{ss} term to the parasitic inversion voltage will be independent of SiO_2 thickness.

5.4 Results pertaining to p-type substrates

The substrate conductivity type does not appear directly in the model that has been proposed for the magnitude and origin of Q_{ii}, and all of the results presented so far have been for n-type substrates. Since the silicon substrate will be intrinsic at 900°C, the deposition temperature of the Al_2O_3, the voltage drop across the oxide V_c will be the same for both n-type and p-type substrates and, thus, Q_{ii} at 900°C should also be independent of the conductivity type of the substrate. If, during the cool down after Al_2O_3 deposition, Q_{ii} is frozen in at a temperature at which the silicon is still intrinsic, then the value of Q_{ii} measured at room temperature should not depend on whether the substrate is n-type or p-type. Results obtained with ⟨100⟩, p-type substrates are presented below.

A plot for p-type substrates similar to that of Fig. 11 (for n-type substrates) is given in Fig. 16, where ΔV_{FB} is plotted as a function of

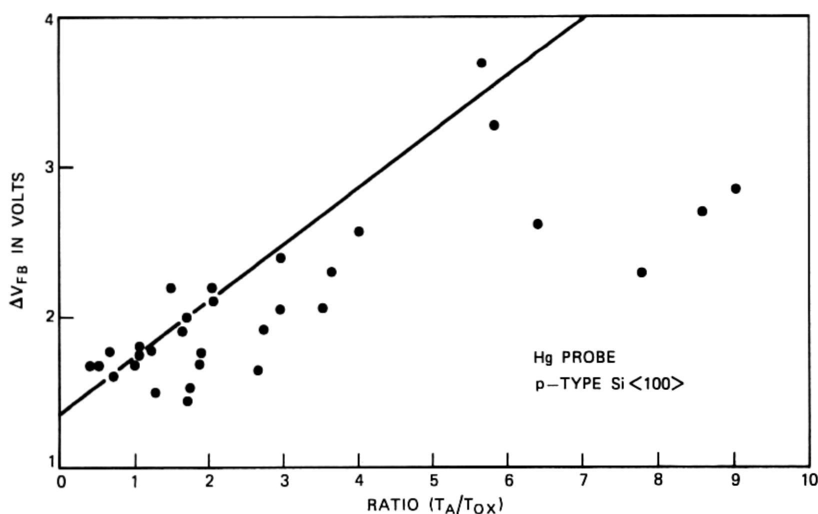

Fig. 16—Plot of the corrected differential flatband voltage as a function of the ratio of Al_2O_3 thickness to SiO_2 thickness on p-type, ⟨100⟩, Si substrates. The solid line is taken from Fig. 11.

T_A/T_{ox}. The solid line corresponds to the linear fit of the data of Fig. 11. Although there is general agreement between the results for the n-type substrate (solid line) and this experimental data, the large amount of scatter in the data must be recognized. Figure 17 is a plot of the single-insulator flatband voltage for the p-type substrates after the Al_2O_3 etch-off. The $(\phi_{m,ox} - \phi_s)$ value was obtained by etch-back experiments, as outlined previously. Here again, a large amount of scatter in the data is evident.

The variations in the above sets of data are not random scatter, but are due to some mechanism unique to the p-type substrates. In Fig. 18, the single-insulator flatband voltage V_{FB}(S.I.) is plotted as a function of T_A for n-type samples after Al_2O_3 etch-off, and it is clear that no dependence on T_A or T_{ox} is evident. In Fig. 19, similar data are plotted for the p-type samples and it is evident that in this case there is a dependence on T_A, but again, no dependence on T_{ox}. For both cases, the conclusions regarding T_{ox} are obtained from the points in Figs. 18 and 19, which explicitly denote points of constant T_{ox}. Although a detailed explanation of this effect cannot be given, it is felt that this effect is due to the fact that boron-doped p-type wafers were used in the experiment. It is known that boron will greatly out-diffuse from a silicon substrate into an SiO_2 layer in the presence of a high-temperature, hydrogen-containing ambient.[16,17] Additionally, the introduction of this impurity into the SiO_2 may enhance its conduc-

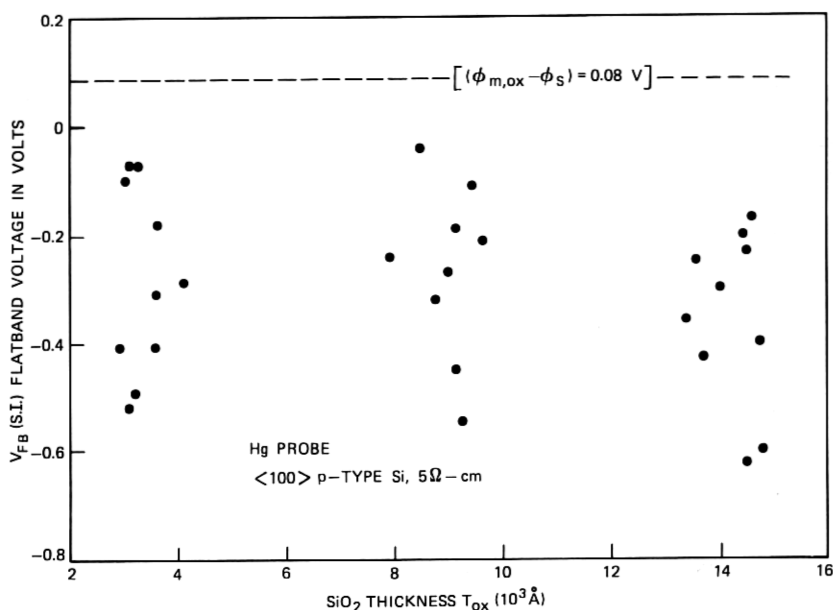

Fig. 17—Plot of the single-insulator flatband voltage after Al_2O_3 deposition and etch-off as a function of the SiO_2 thickness for *p*-type, ⟨100⟩, Si substrates.

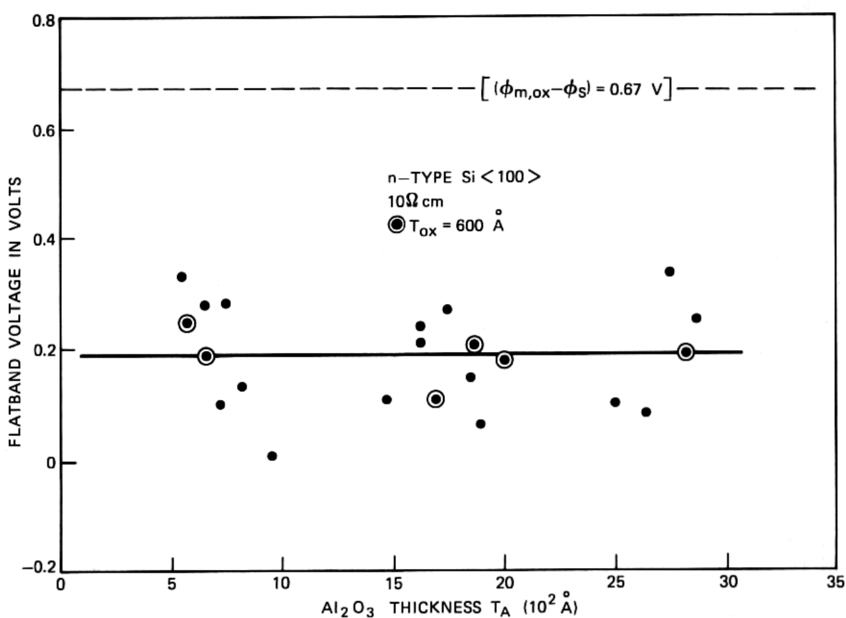

Fig. 18—Plot of the single-insulator flatband voltage after Al_2O_3 deposition and etch-off as a function of the Al_2O_3 thickness for *n*-type, ⟨100⟩, Si substrates.

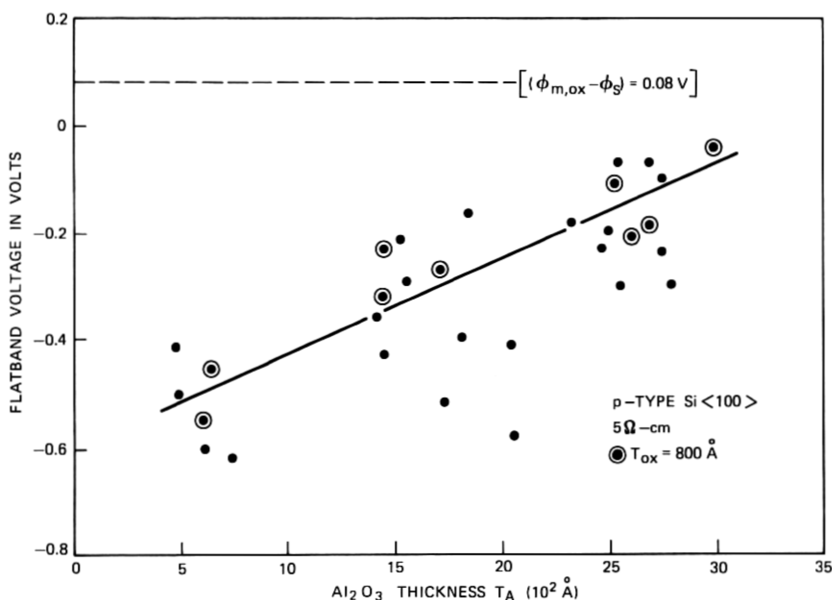

Fig. 19—Plot of the single-insulator flatband voltage after Al_2O_3 deposition and etch-off as a function of the Al_2O_3 thickness for p-type, ⟨100⟩, Si substrates.

tivity at high temperature. The net result will be a drop in the effective stress voltage V_c across the SiO_2 layer as a function of Al_2O_3 deposition time* and a lowering of the Q_{ii} and Q_{ss} term.

This hypothesis is consistent with the following data. In Fig. 20, distributions of the potential drop v_o due to the induced Q_{ss} term (see eqs. 19 and 20) are plotted for both the n-type and p-type ⟨100⟩ samples. It is observed that

(*i*) Lower voltage drops for p-type samples occur than observed for the n-type samples (the lower values are correlated to the thicker Al_2O_3 deposition).

(*ii*) No zero (or negative) voltage drops occur.

(*iii*) The upper range of v_o for the p-type samples (the lowest SiO_2 conductivity region), are bounded by the v_o values observed for the n-type samples.

One final point can also be made to support the hypothesis. It is possible to calculate Q_{ii} values from the experimental data (via eqs. 10 and 18) if an intercept voltage value (i.e., $T_A = 0$) is assumed; and from the experimental data for n-type samples, an intercept value of

---

* In all experiments, the Al_2O_3 deposition rate was a constant (75 Å/min.).

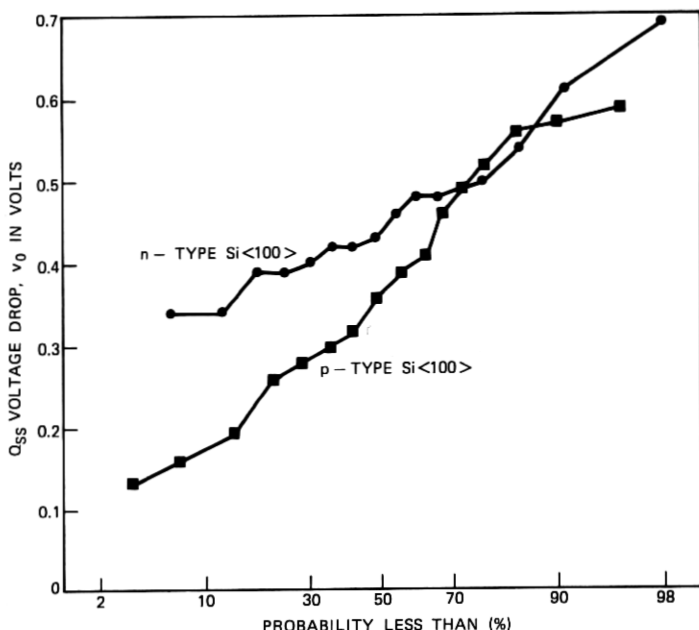

Fig. 20—Distribution plot of the single-insulator flatband voltage observed on n-type and p-type, $\langle 100 \rangle$, Si substrates after Al_2O_3 deposition and etch-off.

1.25 volts was obtained. Additionally, Q_{ss} values for each sample may be calculated. If the above hypothesis concerning a lowering of V_c is correct, then the ratio of Q_{ii} and Q_{ss} (given in eqs. 20 and 23) should be independent of the absolute magnitude of V_c for $\langle 100 \rangle$ substrates in which Q_{sso} is negligible. That is,

$$Q_{ss} = \epsilon_{ox} v_o / T_{ox} = \epsilon_{ox} \alpha^{-1} V_c / T_{ox}$$

and (25)

$$Q_{ii}/Q_{ss} = \alpha.$$

Figure 21 is a plot of Q_{ii} vs Q_{ss} for both the n-type and p-type samples. It is noted that a linear relationship exists for both sets of data with α the same for both ($\alpha \approx 2.5$). The several data points that deviate from the linear relation are associated with very small Q_{ss} and Q_{ii} values, and the deviation is most likely due to small errors in flatband voltage measurements.

5.5 *Results pertaining to observed potential jumps*

Extrapolating the linear relationships in Figs. 9, 11, and 12 to $T_A = 0$ gives a value:

$$(\phi_{m,A} + \phi_{ii} - \phi_{m,ox}) + V_m \triangleq \Delta\phi + V_m \simeq 1.25 \text{ volts.} \qquad (26)$$

While the experiments cannot determine the relative contributions of V_m and $\Delta\phi$ to the intercept value, it is worth pointing out the consequences of the two limiting possibilities. First, if V_m is zero, then $\Delta\phi$ is non-zero and equal to 1.25 volts. This implies that the work function model for barrier heights must be incorrect (otherwise $\Delta\phi = 0$). The second limiting possibility is that $\Delta\phi = 0$ and V_m is non-zero. In this case, there must be a 1.25-volt band-bending effect at the outer Al_2O_3 interface. Although we have not been able to perform an experiment that unequivocally separates the contributions of $\Delta\phi$ and V_m to the intercept value, it is worthwhile to consider some additional items of relevant experimental information.

First, it was stated previously that all samples are fabricated with a deposited SiO_2 layer on top of the Al_2O_3 layer. An etch-back experiment was conducted on the deposited SiO_2 (using n-type Si, ⟨100⟩, $T_{ox} = 600$ Å, $T_A = 500$ Å) and the flatband voltage was measured as a function of the equivalent SiO_2 thickness T_{eq}:

$$T_{eq} = T_{ox} + (\epsilon_{ox}/\epsilon_A)T_A + T_{SiO_2}, \tag{27}$$

where T_{SiO_2} equals the deposited SiO_2 thickness. The results of this

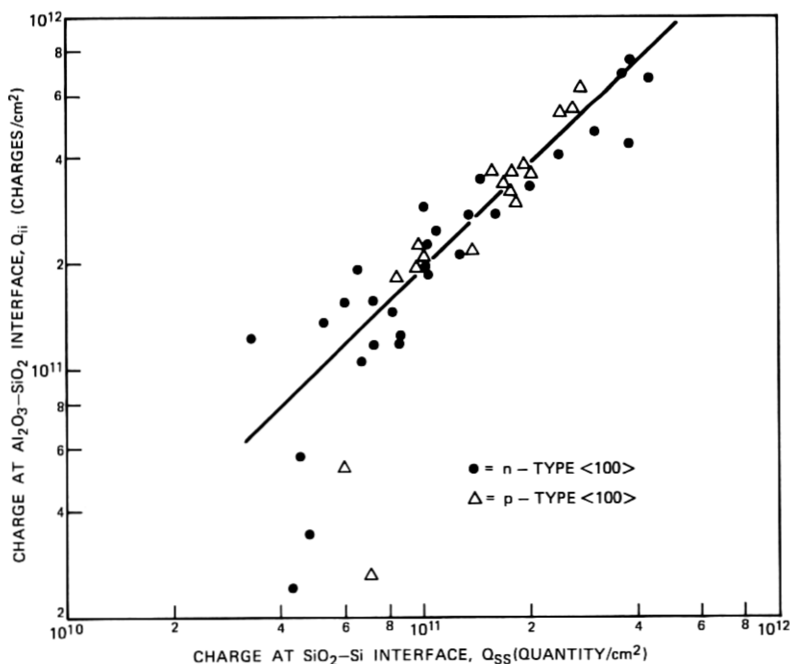

Fig. 21—Plot of Q_{ii}, the charge at the Al_2O_3/SiO_2 interface, versus Q_{ss}, the charge at the SiO_2/Si interface, for both n-type and p-type, ⟨100⟩, Si substrates.

experiment are plotted in Fig. 22. It is evident from the linearity of the flatband voltage that no significant charge density is present in the bulk of this deposited SiO_2. It is interesting to note that a positive potential jump of 1.22 volts in the flatband voltage is associated with the outer Al_2O_3/SiO_2 deposited interface (using the Hg metal electrode). This value is close to the 1.25-volt potential jump associated with the inner Al_2O_3/SiO_2 (thermal) interface.

It is straightforward to show that the potential jump observed in Fig. 22 is given by

$$PJ = (\phi_{m,A} + \phi_{ii} - \phi_{m,ox}) \tag{28}$$

if it is assumed that there is no change in the charge distribution in the Al_2O_3 film when the deposited SiO_2 is completely removed, and that the barrier height of metal-to-deposited-SiO_2 is the same as the barrier height of metal-to-thermal-SiO_2. With these assumptions, the conclusion follows that $V_m \simeq 0$ and $\Delta\phi \simeq 1.25$ volts.

Second, measurements were also made with titanium-aluminum evaporated electrodes. The double-insulator flatband voltage for this metallization system is plotted in Fig. 23 as a function of the Al_2O_3 thickness T_A for a constant SiO_2 thickness $T_{ox} \approx 1200$ Å (n-type Si, $\langle 100 \rangle$). It is evident that the scatter in the data is much greater than that found for the Hg metallization. Attempts to refine the data proved

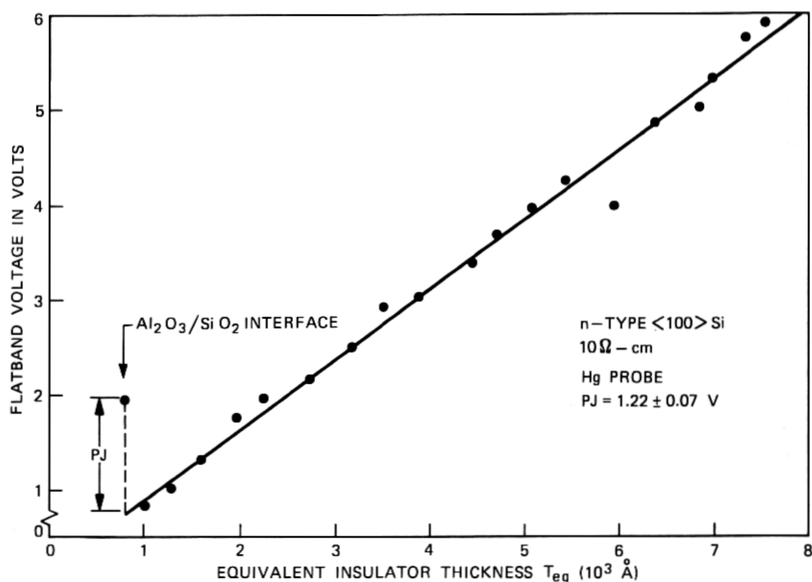

Fig. 22—Plot of the triple-insulator flatband voltage, obtained by means of an etch-back experiment, as a function of the equivalent insulator thickness.

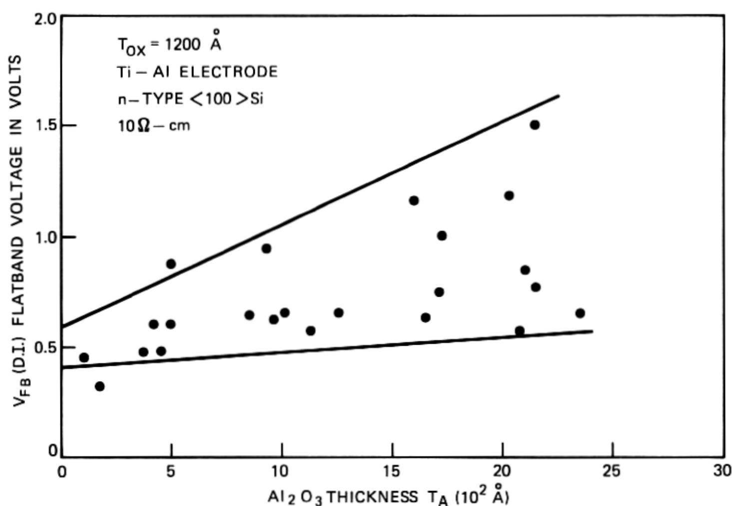

Fig. 23—Plot of the titanium-gate double-insulator flatband voltage as a function of the Al_2O_3 thickness for a constant SiO_2 thickness (T_{ox} = 1200 Å) on n-type, ⟨100⟩, Si substrates.

fruitless due to the additional scatter observed in the single-insulator (SiO_2) flatband voltages (see Fig. 24).

Some general comments can be made, however, concerning these data. The scatter in the double-insulator flatband voltage (Fig. 23) decreases with descreasing Al_2O_3 thickness, indicating that an uncontrolled charging effect must take place in the Al_2O_3 during the

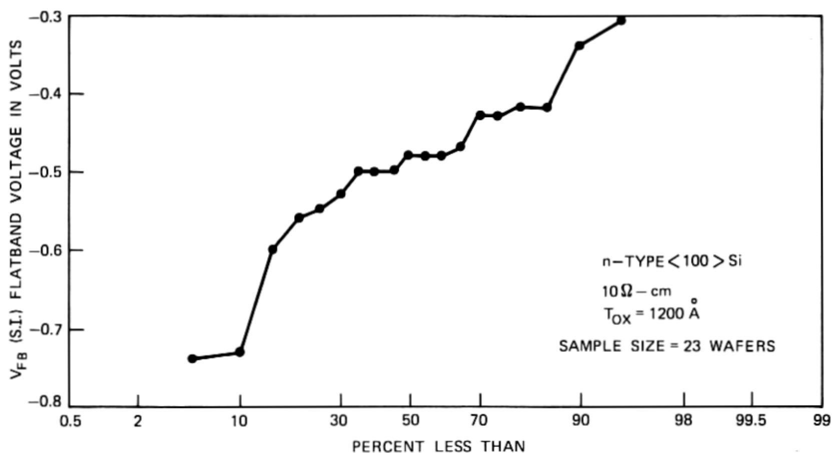

Fig. 24—Distribution plot of the titanium-gate single-insulator flatband voltage after Al_2O_3 etch-off as observed on the samples reported in Fig. 23.

metal deposition. Extrapolating to $T_A = 0$ implies

$$0.40 \text{ V} \leqslant [V_{FB}(\text{D.I.})|_{T_A=0}] \leqslant 0.60 \text{ volt}. \tag{29}$$

The distribution in the single-insulator flatband voltage V_{FB}(S.I.) can be characterized by (see Fig. 24)

$$\text{Average } V_{FB}(\text{S.I.}) = -0.48 \text{ volt}$$
$$\text{Standard Deviation } V_{FB}(\text{S.I.}) = 0.10 \text{ volt}.$$

Thus, a positive potential jump of 0.98 ± 0.14 volt can be associated with the addition of the Al_2O_3 layer. This value is in reasonable agreement with the previous potential shift results found for the Hg metallization system.

Third, in Ref. 4, the authors find on a V_{FB}(D.I.) versus T_A plot for various T_{ox} values an intercept value of −0.80 volt at $T_A = 0$. This result, obtained on 2-ohm-cm, p-type, ⟨100⟩, Si substrates, is interpreted by the authors to be the expected metal-to-silicon work function difference when using aluminum electrodes, a conclusion that may not be valid since Q_{ss} measurements after Al_2O_3 deposition were not reported. We shall now show that the results in Ref. 4 are in excellent agreement with our results by taking the results we have obtained with a Hg electrode and converting them to the results we would have obtained if we had used an Al electrode.

To explicitly denote the use of a Hg electrode, eq. (26) is rewritten as

$$(\phi_{\text{Hg, A}} + \phi_{ii} - \phi_{\text{Hg}, ox}) + V_m = 1.25 \text{ V} \tag{30}$$

and from our measurements on p-type material

$$\phi_{\text{Hg}, ox} - \phi_s = 0.08 \text{ V}. \tag{31}$$

The difference in barrier heights between Hg and Al on the type of Al_2O_3 studied in this paper has been reported by Nigh[18] and is given by

$$\phi_{\text{Hg, A}} - \phi_{\text{Al, A}} = 1.7 \text{ V}. \tag{32}$$

Combining eqs. (30), (31), and (32) yields

$$(\phi_{\text{Al, A}} + \phi_{ii} - \phi_s) + V_m = -0.37 \text{ V}. \tag{33}$$

The intercept value for $T_A = 0$ predicted by (14) is given by

$$\text{Intercept } (T_A = 0) = (\phi_{\text{Al, A}} + \phi_{ii} - \phi_s) + V_m - \frac{Q_{ss}T_{ox}}{\epsilon_{ox}}. \tag{34}$$

Using the values $v_o = 0.38$ volt and $Q_{sso} = 0$ for ⟨100⟩ material in eq. (20), and combining eqs. (20), (33), and (34) yields

$$\text{Intercept } (T_A = 0) = -0.75 \text{ V}.$$

Thus, our corresponding intercept value for Al electrodes is almost identical to that reported in Ref. 4, and it strongly implies that the electrical properties of the different Al_2O_3/SiO_2 films which determine the flatband voltage in MOS structures are identical. More specifically, it indicates that the Q_{ss} dependence on T_{ox} reported in this paper is also true for the structures studied in Ref. 4, and that the value of $\Delta\phi + V_m$ in both cases is the same.

VI. SUMMARY AND DISCUSSION

By varying the thicknesses of both insulators in a silicon/SiO_2/Al_2O_3/mercury MOS structure and accurately measuring changes in flatband voltage, we have established that a net negative space charge exists near the SiO_2/Al_2O_3 interface, which is spatially constrained to a region much less than 500 Å thick. The magnitude of this negative charge varies inversely with SiO_2 thickness and is the same for both ⟨100⟩ and ⟨111⟩ oriented n-type and p-type silicon substrates. These results are consistent with a model for space-charge formation based on work by Simmons on metal-insulator-metal structures.[6] At the elevated temperature (900°C) of Al_2O_3 deposition, the Al_2O_3 is a good enough conductor that thermal equilibrium is established. Since the electrostatic screening or Debye length in Al_2O_3 at this temperature is small compared to the Al_2O_3 thickness of interest, the bulk of the Al_2O_3 is at zero electric field, and a Fermi level can be defined that must align with the Fermi level in the silicon substrate. This requires that a fixed "contact potential", experimentally found to be 0.88 volt, must exist across the SiO_2 at 900°C. The electric field associated with this potential generates a net negative space-charge layer near the SiO_2/Al_2O_3 interface. When the structure is cooled to room temperature, the conductivity of the Al_2O_3 reduces to a negligible value and the space charge is frozen in. The net negative charge can thus be considered to be the charge on the SiO_2 capacitance associated with the constant 0.88 volt contact potential.

When the double-insulator flatband voltage is corrected for the independently measured Si/SiO_2 interface charge Q_{ss} and the barrier heights of the single-insulator system, a corrected differential flatband voltage is generated. Extrapolation of this function to zero Al_2O_3 thickness reveals a potential jump of approximately 1.25 volts when using a mercury electrode. Similarly, a potential jump of approximately 1.0 volt is found with titanium-aluminum electrodes. The interfacial barrier energies that contribute to these jumps are shown not to be derivable from a simple work function argument.

The large amount of scatter observed in the data where titanium-aluminum electrodes are used, compared to the very consistent data

obtained with the mercury electrode, implies that thermal evaporation of a metal onto an Al_2O_3 film introduces significant variation in the flatband voltage. This effect is most probably due to a charging phenomena that occurs during the transient heating of the sample during evaporation.

Measurements of Q_{ss} made on samples before and after Al_2O_3 deposition revealed that during this deposition, the value of Q_{ss} was changed. After Al_2O_3 deposition, it was found that Q_{ss} could be written as the sum of two terms. One term was a constant background charge density that was independent of SiO_2 thickness and that had the values of 1.0×10^{11} and 1.0×10^{10} charges/cm^2 for $\langle 111 \rangle$ and $\langle 100 \rangle$ oriented substrates, respectively. The other term was orientation independent and inversely proportional to the SiO_2 thickness, indicating that it is derivable from a constant contact potential that was experimentally determined to be 0.38 volt. Thus, the electric field that exists in the SiO_2 during the deposition of the Al_2O_3 determines not only Q_{ii} but also a portion of Q_{ss}.

The proposed charging model was also found to be correct for p-type substrates except that an additional effect was uncovered in that the effective contact potential decreased with increasing Al_2O_3 thickness. This effect may be due to boron penetration of the thermal SiO_2 layer and an associated increased electrical conductivity at high temperature.

According to the model presented, a contact potential exists across the SiO_2 at the Al_2O_3 deposition temperature, which results in an electric field in a direction to drive mobile positive ions away from the Si/SiO_2 interface. This means that if some mechanism exists for either removing or immobilizing these positive ions when they reach the SiO_2/Al_2O_3 interface, the Al_2O_3 deposition is expected to stabilize the MIS system against ionic drifts. Such a mechanism may indeed be present since HCl, a by-product of the Al_2O_3 formation reaction, is known to be an excellent sodium getter. While the importance of this electric field in accounting for the stability of the SiO_2/Al_2O_3 system is not presently clear, it seems reasonable to assume that net positive charge at the insulator-insulator interface would make it much more difficult to remove or immobilize positive ions in the SiO_2 during second insulator deposition, since the positive ions would then tend to drift to the Si/SiO_2 interface.

Since the presented model for space-charge layer formation at insulator-insulator interfaces is relatively insensitive to the nature of the deposited insulator, provided the assumption of thermal equilibrium at the deposition temperature is correct, considerations similar to those given in this paper for the SiO_2/Al_2O_3 system should apply to other SiO_2/deposited insulator systems.

VII. ACKNOWLEDGMENTS

The authors acknowledge L. P. Adda and H. E. Nigh for many interesting discussions concerning the electrical characteristics of the $Al_2O_3/SiO_2/Si$ structure. In addition, the authors thank E. G. Parks and J. J. Nolen for their help in fabricating and measuring the many samples used in this study.

REFERENCES

1. S. K. Tung and R. E. Caffrey, "The Deposition of Oxide on Silicon by the Reaction of a Metal Halide with a Hydrogen-Carbon Dioxide Mixture," Trans. Met. Soc., AIME, *233* (March 1965), pp. 572–577.
   H. E. Nigh, J. Stach, and R. M. Jacobs, "A Sealed Gate IGFET," IEEE Trans. El. Dev., *14*, No. 9 (September 1967), p. 631.
2. J. T. Clemens and E. F. Labuda, "Semiconductor Silicon 1973," edited by H. R. Huff and R. R. Burgess, Electrochemical Society, Princeton, N. J., pp. 779–790.
3. M. P. Lepselter, "Beam Lead Technology," B.S.T.J., *45*, No. 2 (February 1966), pp. 233–253.
4. J. A. Aboff, D. R. Kerr, and E. Bassous, "Charge in SiO_2/Al_2O_3 Double Layers on Silicon," J. Electrochem. Soc., *120*, No. 8 (August 1973), pp. 1103–1106.
5. E. F. Labuda, J. T. Clemens, and C. N. Berglund, IEEE Dev. Res. Conf., University of Michigan, Ann Arbor, June 28-July 1, 1971.
6. J. G. Simmons, "Electronic Conduction Through Thin Insulating Films," *Handbook of Thin Film Technology*, edited by L. I. Maissel and R. Glang, Chapter 14, New York: McGraw-Hill, 1970.
7. C. N. Berglund and R. J. Powell, "Photoinjection into SiO_2: Electron Scattering in the Image Force Potential Well," J. Appl. Phys., *42*, No. 2 (February 1971), pp. 573–579.
   C. N. Berglund and R. J. Powell, "Photoinjection Studies of Charge Distributions in Oxides of MOS Structures," J. Appl. Phys., *42*, No. 11 (October 1971), pp. 4390–4397.
8. D. A. Mehta, S. R. Butler, and F. J. Feigl, "Electronic Charge Trapping in Chemical Vapor-Deposited Thin Films of Al_2O_3 on Silicon," J. Appl. Phys., *43*, No. 11 (November 1972), pp. 4631–4638.
9. J. J. Curry and H. E. Nigh, "8th Annual Proceedings Reliability Physics," IEEE (April 7–10, 1970), p. 29.
10. R. H. Walden and R. J. Strain, "8th Annual Proceedings Reliability Physics," IEEE (April 7–10, 1970), p. 23.
11. R. Hammer, "A Mercury Contract Probe for MOS Measurements on Oxidized Silicon," Rev. Sci. Instr., *41*, No. 2 (February 1970), pp. 292–293.
12. A. S. Grove, *Physics and Technology of Semiconductor Devices*, Chapter 9, New York: John Wiley & Sons, 1967.
13. H. Kolter, J. J. H. Schatorje, and E. Kooi, "Electric Double Layers in MIS Structures with Multilayered Dielectrics," Philips Res. Repts., *26* (1971), pp. 181–190.
14. B. E. Deal, M. Sklar, A. S. Grove, and E. H. Snow, "Characteristics of the Surface State Charge (Q_{SS}) of Thermally Oxidized Silicon," J. Electrochem. Soc., *114*, No. 3 (March 1967), pp. 266–273.
15. A. Goetzberger and H. E. Nigh, "Surface Charge After Annealing of $Al/SiO_2/Si$ Structures Under Bias," Proc. IEEE, *54*, No. 10 (October 1966), p. 1454.
16. A. S. Grove, O. Leistiko, and C. T. Sah, "Redistribution of Acceptor and Donor Impurities During Thermal Oxidation," J. Appl. Phys., *35*, No. 9 (September 1964), pp. 2695–2701.
17. B. E. Deal, A. S. Grove, E. H. Snow, and C. T. Sah, "Observation of Impurity Redistribution During Thermal Oxidation of Silicon Using the MOS Structure," J. Electrochem. Soc., *112*, No. 3 (March 1965), pp. 308–314.
18. H. E. Nigh, Proc. of Intl. Conf. on Properties and Use of MIS Structures, Grenoble, France (June 17–20, 1969), pp. 77–88.